npj | aging

Article

Published in partnership with the Japanese Society of Anti-Aging Medicine

https://doi.org/10.1038/s41514-026-00332-6

Parkin deficiency impairs female fertility, oocyte development, fertilization and mitochondrial function in mice

Check for updates

Michelle Volovsky[1,5], Adolfo Rodríguez-Eguren[1,2,5], Yagmur Ergun[1,5], Raziye Melike Yildirim[1], Gizem Nur Sahin[1], Rolando Garcia Milian[3], Sameet Mehta[4], Lavinia Turanli[1], Irene Cervelló[2], Richard Scott[1] & Emre Seli[1] ✉

Parkin, a mitochondrial E3 ubiquitin ligase, plays a central role in mitophagy and cellular homeostasis. Although well studied in neurobiology, its role in female reproduction remains unclear. This study investigated the role of Parkin on female fertility using young (2–3 months old) and older (9–10 months old) mice with a global germline Parkin deletion. Parkin knockout (KO) females exhibited significantly reduced fertility with total pups per female lower in KO mice (16.0 ± 1.53) compared to wild type (WT) (22.33 ± 0.67; $p = 0.02$). In young mice, GV oocyte yield was significantly reduced in KO (30.0 ± 1.53) compared to WT (52.7 ± 6.96; $p = 0.03$), as was MII oocyte count (7.7 ± 0.67 vs. 22.3 ± 0.88; $p = 0.0002$). In older mice, similar trends were observed. Fertilization rates were significantly lower in KO mice compared to WT (36.2 ± 8.1% vs. 61.2 ± 5.5%; $p = 0.03$). RNA sequencing identified multiple differentially expressed genes between KO and WT, with associated pathway changes. These findings indicate that Parkin deficiency impairs oocyte yield, fertilization capacity, and overall fertility, suggesting that Parkin plays a key role in reproductive competence.

The trend of delayed reproduction has become increasingly common, with many women choosing to have children later in life due to career, financial, or personal priorities[1,2]. This delay exacerbates age-related fertility challenges, such as diminished ovarian reserve and increased aneuploidy rates[3,4]. Understanding the molecular mechanisms that underlie reproductive aging, such as those involving mitochondrial quality control, is crucial to addressing the growing challenge of infertility in the context of delayed reproduction.

Mitochondrial function is central to a broad range of cellular processes, including ATP production, regulation of apoptosis, and maintenance of oxidative balance[5,6]. Disruption of mitochondrial homeostasis has been linked to multiple pathologies, from neurodegenerative disorders to metabolic syndromes, many of which are exacerbated by age[7]. One key player in mitochondrial quality control is Parkin (encoded by the PARK2 gene), an E3 ubiquitin ligase implicated in autosomal recessive and early onset forms of Parkinson's disease[8,9]. Under conditions of mitochondrial stress or depolarization, Parkin, together with the PTEN Induced Kinase 1 (PINK1), labels damaged mitochondria for autophagic clearance[9–11]. PINK1 accumulates on the outer mitochondrial membrane and phosphorylates Parkin, enhancing its activity and tagging compromised mitochondria for autophagic degradation. Notably, a non-phosphorylated form of Parkin can maintain normal mitochondrial function and morphology under PINK1 deficiency, underscoring the importance of Parkin independent of PINK1 phosphorylation in mitochondrial quality control, particularly as aging impacts mitochondrial integrity.

In addition to its well-documented role in mitophagy, emerging evidence has suggested that Parkin's function extends beyond the nervous system and can influence metabolic homeostasis and cellular stress responses in multiple tissues[12–15]. However, despite mitochondrial quality control being particularly relevant in high energy demand tissues such as gonads, the potential role of Parkin in the female reproductive system remains relatively unexplored.

Oocytes are notably metabolically active, and their progression from the germinal vesicle (GV) stage to the metaphase II (MII) stage requires a strong mitochondrial network to supply adequate ATP and to regulate reactive oxygen species[16–20]. Moreover, the maintenance of mitochondrial integrity and capacity for dynamic remodeling are essential for oocyte competence and overall reproductive success[18–20].

[1]Department of Obstetrics, Gynecology, and Reproductive Sciences, Yale School of Medicine, New Haven, CT, USA. [2]IVIRMA Global Research Alliance, IVI Foundation, Instituto de Investigación Sanitaria La Fe (IIS La Fe), Valencia, Spain. [3]Bioinformatics Support Hub, Cushing/Whitney Medical Library, Yale School of Medicine, New Haven, CT, USA. [4]Yale Center for Genome Analysis, Department of Genetics, Yale School of Medicine, New Haven, CT, USA. [5]These authors contributed equally: Michelle Volovsky, Adolfo Rodríguez-Eguren, Yagmur Ergun. ✉e-mail: emre.seli@yale.edu

Table 1 | Subfertility in Parkin KO mice

Fertility assessment of PARKIN KO females						
Genotype	*n*	Litters	Pups	Pups per litter	Litter per female	Pups per female
WT	3	11	67	6.09 ± 0.28	3.67 ± 0.33	22.33 ± 0.67
KO	3	9	48	5.22 ± 0.76	3.00 ± 0.00	**16.00 ± 1.53***

Fertility in female Parkin KO and WT mice (2 months old, $n = 3$ for each genotype) was assessed by mating them with WT males of proven fertility (male/female; 1:1) for 12 weeks. Data presented as means ± SEM, with*$p < 0.05$ (in bold) using an unpaired *t*-test.

These functions are modulated by quality control systems that ensure coordinated degradation, repair and structural adaptation of mitochondria. Some key regulators include CLPP, a mitochondrial matrix protease responsible for eliminating misfolded proteins, and the mitofusins MFN1 and MFN2, which mediate outer mitochondrial membrane fusion, a process that supports content exchange and metabolic plasticity[21–24]. Disruption of these pathways has been demonstrated to result in subfertility, impaired oocyte development, reduced fertilization and compromised embryonic development[25–27]. It follows that other factors modulating mitochondrial health, such as Parkin-mediated mitophagy, could impair mitochondrial turnover and influence reproductive potential. However, the specific consequences of Parkin depletion on oocyte maturation, follicle development, fertilization, and overall fertility, have not been well studied.

To address this gap, we examined the hypothesis that Parkin knockout (KO) mice exhibit compromised female fertility, potentially associated with impaired mitochondrial quality control in the ovary. We evaluated multiple reproductive parameters, including the number of GV and MII oocytes, fertilization, follicle counts in ovarian tissue, transcriptomic changes (via RNA sequencing) and mitochondrial function in oocytes. By elucidating the role of Parkin in ovarian physiology, this research aims to deepen our understanding of the molecular mechanisms behind female infertility and to highlight mitochondrial quality control as a critical determinant of reproductive success.

Results

Deletion of Parkin results in subfertility

To evaluate fertility, female Parkin KO and wild-type (WT) mice were housed with proven fertile males for a continuous 12-week breeding period. Parkin KO females produced significantly fewer pups per female over the 12-week period compared to WT counterparts (16.00 ± 1.53 vs. 22.33 ± 0.67; $p = 0.02$), indicating a marked reduction in overall fertility (Table 1). Additionally, the estrous cycle was staged using uterine lavage and noted to be the same length of 4 days through proestrus, estrus, metestrus and diestrus, in both in KO and WT mice (Supplementary Fig. 1).

Parkin deletion causes impaired oocyte development

Assessment of Parkin's role in oocyte development was performed by measuring oocyte yield following superovulation in both young (2–3 months old) and older (9–10 months old) female mice. Germinal vesicle (GV) and metaphase II (MII) oocytes were collected and quantified. In young mice, Parkin KO females exhibited a significant reduction in the average GV oocyte yield per animal compared to WT controls (30.00 ± 1.53 vs. 52.70 ± 6.96; $p = 0.03$), indicating impaired early oocyte growth or follicular response. This deficit was even more pronounced at the MII stage, where average ovulated oocyte counts per animal were markedly lower in KO mice than in WT (7.70 ± 0.67 vs. 22.30 ± 0.88; $p = 0.0002$), suggesting a severe disruption in oocyte maturation or ovulation efficiency (Fig. 1A, C). In older mice, similar trends were observed. GV oocyte counts were reduced in KO mice compared to WT (12.20 ± 1.87 vs. 16.30 ± 1.28; $p = 0.09$), and MII oocyte counts also trended lower (4.50 ± 1.31 vs. 6.00 ± 1.46; $p = 0.46$) (Fig. 1B, D).

Reduced fertilization in Parkin deficient mice

To assess the impact of Parkin deletion on fertilization, in vitro fertilization (IVF) was performed using MII oocytes collected from superovulated Parkin KO and WT females per established protocols[28]. Fertilization was confirmed by the presence of two pronuclei (2PN) the following morning. Across all age groups, average fertilization rates per animal were significantly lower in Parkin KO mice compared to WT controls (36.2 ± 8.1% vs. 61.2 ± 5.5%; $p = 0.03$), indicating a substantial impairment in fertilization efficiency in the absence of Parkin (Fig. 1G). When stratified by age, a similar pattern was observed in both young and older cohorts. In young mice, KO oocytes demonstrated reduced fertilization rates compared to WT (35.0 ± 17.6% vs. 58.7 ± 4.3%; $p = 0.26$), which persisted in older mice (37.3 ± 4.3% in KO vs. 65.0 ± 15.0% in WT; $p = 0.11$) (Fig. 1E, F).

Follicle development

To determine whether Parkin deletion affects follicle development or ovarian reserve, we quantified follicle numbers across developmental stages in both young and older female mice. Histological analysis was performed on ovarian sections from Parkin KO and WT mice, and follicles were classified as primordial, primary, secondary, pre-antral, or antral based on established morphological criteria[29,30]. In young mice, no significant differences were observed between KO and WT groups across any follicle class (Fig. 2A, B). Likewise, in older mice, follicle counts remained comparable between genotypes (Fig. 2C, D), suggesting that Parkin deficiency does not impact the composition of the ovarian follicle pool.

Gene expression is altered in Parkin deficient oocytes

RNA sequencing of pooled GV oocytes from Parkin KO and WT mice at 3 months, 6 months, and 9 months (3 KO and 3 WT per group) identified transcriptional changes between KO and WT at all ages. In the younger group (Fig. 3), 20 differentially expressed genes (DEGs) were identified, with 12 upregulated and 8 down-regulated genes in Parkin KO mice compared to WT controls (Fig. 3A). Of these, some of the top upregulated DEGs included *Gm9825*, an RNA binding protein gene, *Prss30*, a gene thought to enable endopeptidase activity and sodium channel regulator activity, and *Sytl3*, associated with calcium-dependent phospholipid binding activity (Fig. 3B, C). The most notably down-regulated gene was *Dcpp3*, encoding a protein predicted to be active in the extracellular space and notably expressed in embryos. Pathway enrichment analysis revealed significantly affected pathways, including those relating to eukaryotic translation initiation, elongation and termination, mitochondrial RNA modification and degradation, and ribosomal quality control signaling (Fig. 3D).

By 6 months (Fig. 4), the number of DEGs increased between the Parkin KO and WT groups, with a total of 38 genes noted, 18 up-regulated and 20 down-regulated (Fig. 4A). Once again, *Gm9825* and *Prss30* were among the genes most significantly upregulated, along *with Hmga1−rs1*, a gene associated with several functions, including DNA binding activity, catalytic activity and nuclear retinoid X receptor binding activity (Fig. 4B). In this age group, *Dcpp3* was again observed amongst the most down-regulated genes (Fig. 4C). Pathway analysis identified alterations in pre-mRNA processing, cell junction organization, and fatty acid oxidation pathways (Fig. 4D).

A further increase in DEGs was observed at 9 months (Fig. 5). There was a total of 71 DEGs, with 31 genes up-regulated and 40 down-regulated (Fig. 5A). Consistent with findings at 3 and 6 months, the genes upregulated included *Gm9825*, *Prss30* and *Hmga1−rs1* in KO mice compared to WT, while *Dcpp3* was the most down-regulated transcript (Fig. 5B, C). Pathway analysis in 9-month mice similarly revealed impacts on pre-mRNA processing and fatty acid oxidation pathways, as well as genes expression changes in NADH repair, glycolysis, gluconeogenesis and transcriptional regulation pathways (Fig. 5D).

Mitochondrial function

To assess the impact of Parkin deletion on mitochondrial function, mitochondrial reactive oxygen species (ROS) and membrane potential ($\Delta\Psi m$) in

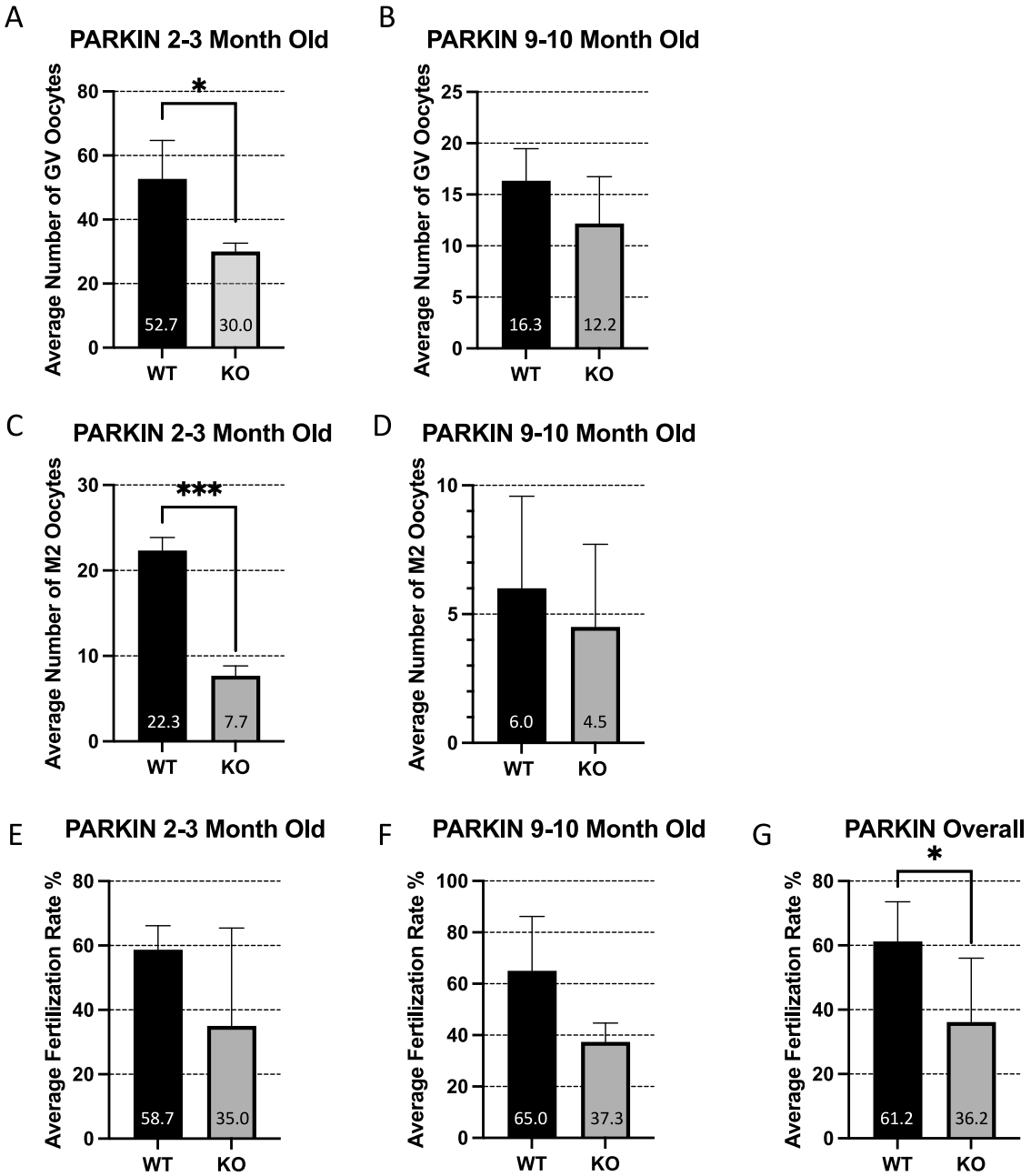


Fig. 1 | Impaired oocyte development and fertilization in Parkin KO mice. **A** Number of Germinal vesicle (GV) oocytes in young KO and WT mice (30.00 ± 1.53 vs. 52.70 ± 6.96; $p = 0.03$, $n = 3$ per group [28, 29, 33 per individual mouse] vs. [54, 40, 64 per individual mouse], respectively) and in (**B**) older KO and WT mice (12.20 ± 1.87 vs. 16.30 ± 1.28; $p = 0.09$, $n = 6$ per group [4, 12, 18, 13, 12, 14 per individual mouse] vs. [11, 20, 18, 15, 16, 18 per individual mouse], respectively). **C** Number of metaphase II (MII) oocytes in young KO and WT mice (7.70 ± 0.67 vs. 22.30 ± 0.88; $p = 0.0002$, $n = 3$ per group [7, 9, 7 per individual mouse] vs. [21, 24, 22 per individual mouse], respectively) and in (**D**) older KO and WT mice (4.50 ± 1.31 vs. 6.00 ± 1.46; $p = 0.46$, $n = 6$ per group [2, 5, 8, 0, 8, 4 per individual mouse] vs. [8, 12, 6, 4, 2, 4 per individual mouse], respectively). **E** Fertilization rates (%) in young (35.0 ± 17.6% vs. 58.7 ± 4.3%; $p = 0.26$, $n = 3$ per group), **F** older (37.3 ± 4.3% in KO vs. 65.0 ± 15.0% in WT; $p = 0.11$, $n = 3$ per group) and **G** all aged mice (36.2 ± 8.1% vs. 61.2 ± 5.5%; $p = 0.03$, $n = 6$ per group). Data presented as means ± SEM, with $^{*}p < 0.05$, $^{***}p < 0.001$ using unpaired t-tests.

GV oocytes was quantified by using staining under live confocal fluorescence imaging under identical settings. Mitochondrial ROS was significantly elevated in Parkin KO GV oocytes compared to WT mice (KO pixel intensity (PI) 22.32 ± 0.42 vs WT PI 19.11 ± 0.74, $p = 0.0003$) (Supplementary Fig2). The ΔΨm was not statistically significantly different between KO GV oocytes and WT GV oocytes (KO ΔΨm 91.12 ± 7.63 vs WT ΔΨm 91.58 ± 6.14, $p = 0.96$) (Supplementary Fig2). These data indicate that Parkin deficiency is associated with increased mitochondrial oxidative stress, without a detectable change in ΔΨm.

Discussion

Our findings using a mouse model with a targeted global germline deletion indicate that Parkin plays a significant role in female fertility. Parkin KO mice exhibited reduced fertility, with fewer pups per female, lower oocyte yields at both GV and MII stages, and decreased fertilization rates compared to WT mice. These results align with the notion that mitophagy is critical for oocyte maturation and reproductive success, given the high energy demands and redox balance requirements of developing oocytes[16–20]. The absence of Parkin appears to

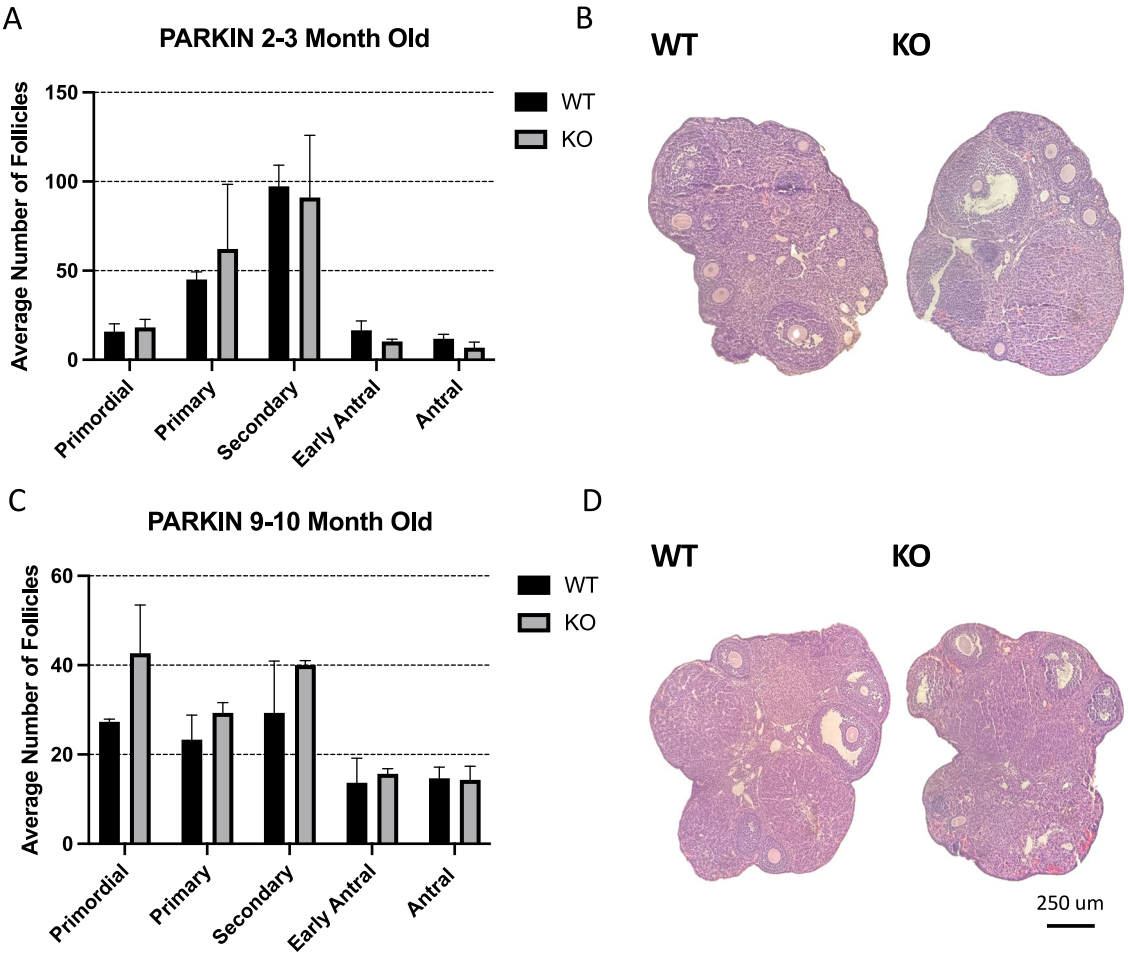


Fig. 2 | Assessment of follicle development in mice with Parkin deletion. Follicle counts in young (**A**) and older (**C**) Parkin KO and WT mice ovaries ($n = 3$ for each genotype per age). Data presented as mean ± SEM. Representative micrographs of young (**B**) and older (**D**) WT and KO mice ovarian sections stained with hematoxylin and eosin at 10×.

disrupt this balance, leading to impaired oocyte development and function.

Interestingly, follicle counts across all stages (primordial, primary, secondary, early antral, antral) were comparable between KO and WT mice, suggesting that Parkin's effects are more pronounced during the later stages of oocyte growth and maturation than during follicle formation or the maintenance of ovarian reserve. This points to the possibility that mitochondrial defects accumulate primarily during the later stages of oocyte development, rather than earlier in folliculogenesis. Consistent with a defect that emerges during growth, mitochondrial function testing indicated a redox imbalance in KO oocytes, with elevated mitochondrial ROS despite preserved ΔΨm. In line with this, RNA sequencing data supports such an interpretation, revealing altered pathways related to ribosomal function, translation and stress response in KO oocytes. Moreover, the number of DEGs between KO and WT oocytes increased with advancing age, suggesting that transcriptional alterations accumulate as a consequence of mitochondrial dysfunction, again compatible with a cumulative oxidative stress burden in Parkin KO oocytes. These changes in gene expression likely contribute to broader cellular stress and metabolic impairment, consistent with the known effect of mitochondrial dysfunction on spindle formation, chromosome segregation, and overall developmental competence[31–33]. Collectively, these disruptions may underlie the observed subfertility, reduced oocyte yield, and lower fertilization rates in Parkin KO mice.

The observation that Parkin's role extends beyond mitophagy to influence regulation of metabolic and stress responses in other tissues aligns with our findings in the ovary[13–15]. Parkin has been shown to maintain metabolic homeostasis in high-energy-demand tissues such as the heart and skeletal muscle, where it mitigates oxidative stress and preserves mitochondrial integrity under metabolic strain[34,35]. This broader role suggests that Parkin may similarly support the ovary's ability to manage metabolic stress, particularly as mice age, when the cumulative burden of mitochondrial dysfunction can exacerbate fertility decline. While compensatory mechanisms may help sustain mitochondrial function in certain ovarian processes, these systems may become less effective with age or under high metabolic demand[14,36]. For example, alternative E3 ligases such as MUL1 have been implicated in mitochondrial quality control independent of the PINK1-Parkin pathway and may partially compensate for Parkin loss in some scenarios, but fail to fully support the ovary's needs as mitochondrial stress accumulates over time[37]. These findings underscore the complexity of mitochondrial quality control in the ovary and its differential impact across physiological states and life stages.

This study has several limitations that should be considered when interpreting our results. First, the number of oocytes obtainable per animal is inherently limited, which reduces the statistical power and may prevent the detection of subtle or stage-specific differences in reproductive outcomes. Second, although RNA sequencing revealed transcriptional changes in pathways like eukaryotic translation and ribosomal function, these findings were not validated at the protein level. The steps that define PINK1-Parkin pathway activation, such as PINK1 accumulation, Parkin recruitment, and downstream ubiquitination, occur primarily in the context of mitochondrial

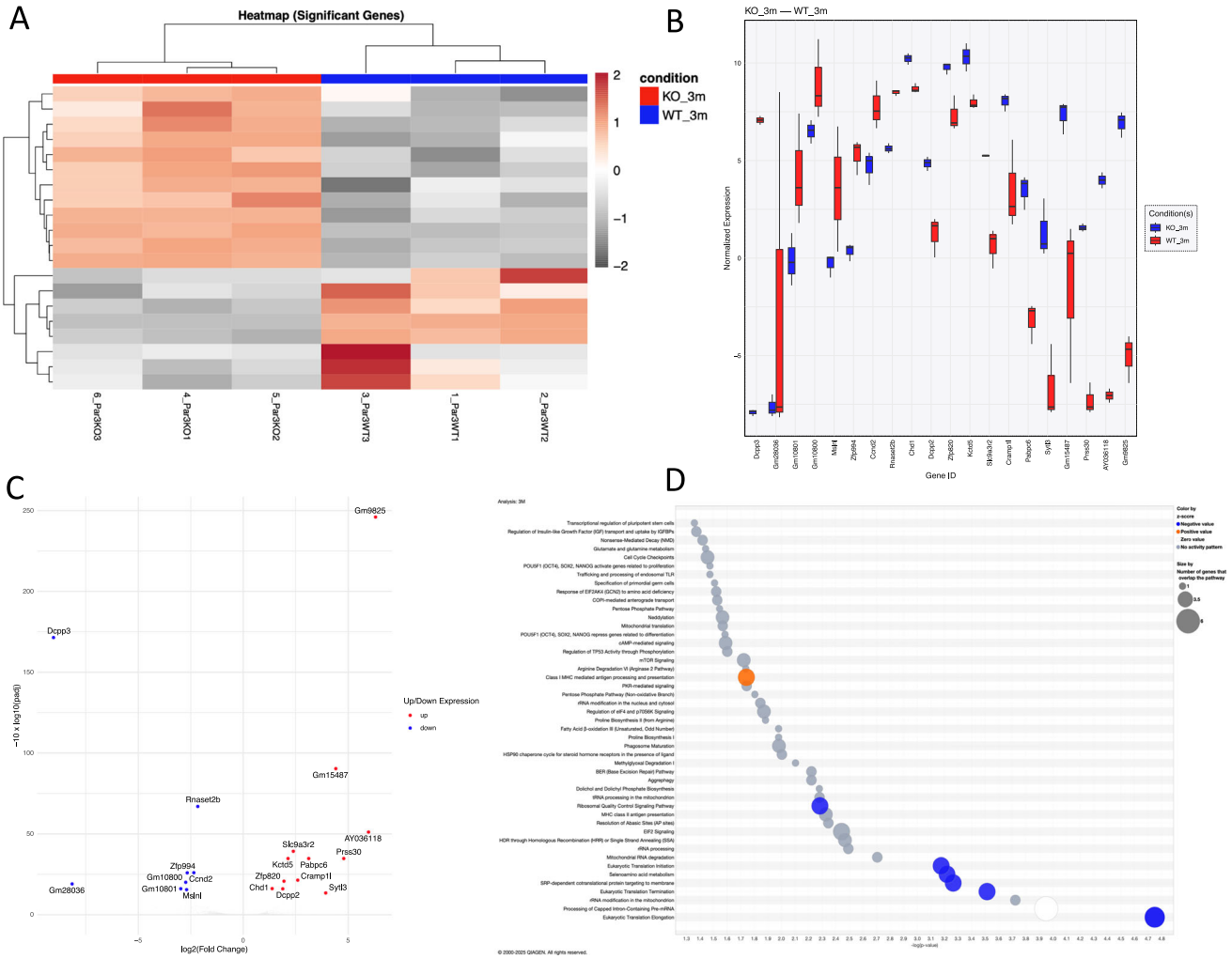


Fig. 3 | Gene expression in Parkin KO oocytes at 3-months-old. A Heatmap illustrating genes differentially expressing between Parkin KO and WT GV oocytes. The color gradient represents normalized expression values, with red indicating higher expression and gray indicating lower expression. **B** Boxplot showing normalized expression levels of the top differentially expressed genes, with red and blue boxes representing WT and KO groups, respectively. **C** Volcano plot showing the distribution of differentially expressed genes between KO and WT oocytes. Each point represents a gene plotted by log2 fold change (x-axis) and -log10 adjusted *p*-value (y-axis). Red dots indicate significantly upregulated genes in KO and blue dots represent down-regulated genes. The remaining non-significant genes are all plotted as smaller gray points that congregate near the middle of the x axis due to low log2 fold change and low -log 10 adjusted *p* values. **D** Bubble plot of Ingenuity Pathway Analysis (IPA) of RNA-seq data from KO vs WT oocytes, highlighting the top affected pathways. Bubble size represents the number of differentially expressed genes overlapping with each pathway. Color indicates predicted activation state: blue for predicted inhibition, orange for predicted activation, gray for no activity pattern detected, and white for pathways with no directionality calculated.

depolarization[9–11]. Therefore, static protein measurements in unstimulated oocytes are unlikely to provide a reliable or biologically meaningful readout of pathway activity. In addition to the already low basal levels of endogenous PINK1 and Parkin[38,39], GV oocytes contain extremely low total protein, making it technically challenging to reliably detect such low abundance proteins. These constraints are common across oocyte studies, which is why many investigations of mitochondrial and quality control pathways in oocytes rely primarily on RNA level analyses and morphological or functional phenotyping[25–27,31,40]. We recognize that emerging ultralow input proteomic platforms may help overcome some of these limitations and future studies using such approaches will be valuable.

Finally, our work was conducted in a mouse model, which, while informative, may not fully capture all aspects of human oocyte biology or mitochondrial quality control mechanisms. As such, caution is warranted when extrapolating these findings to human reproductive physiology. Taken together, these limitations underscore the need for future studies that employ complementary functional assays and further expand on our findings. Furthermore, generating a double KO model for PINK1 and Parkin could provide insights into their collective role in ovarian function. Such a model would help determine whether the combined loss of both proteins exacerbates mitochondrial dysfunction by eliminating potential synergistic effects and reducing compensation through PINK1-dependent pathways[41,42].

This study highlights Parkin's importance in female fertility, with Parkin KO female mice exhibiting subfertility characterized by reduced oocyte yields and fertilization rates together with increased mitochondrial oxidative stress in oocytes. RNA sequencing revealed disruptions in key cellular processes, including protein synthesis and ribosomal function, which may compound age-related reproductive decline. Collectively, these findings position Parkin as a promising avenue for investigation in mitochondria-related infertility, particularly in the context of aging. Further research is warranted to explore its role in enhancing fertility across the reproductive lifespan.

Methods

Animal breeding and genotyping

All animal care, breeding, and experimental protocols were conducted in accordance with the Yale University Animal Research Requirements and

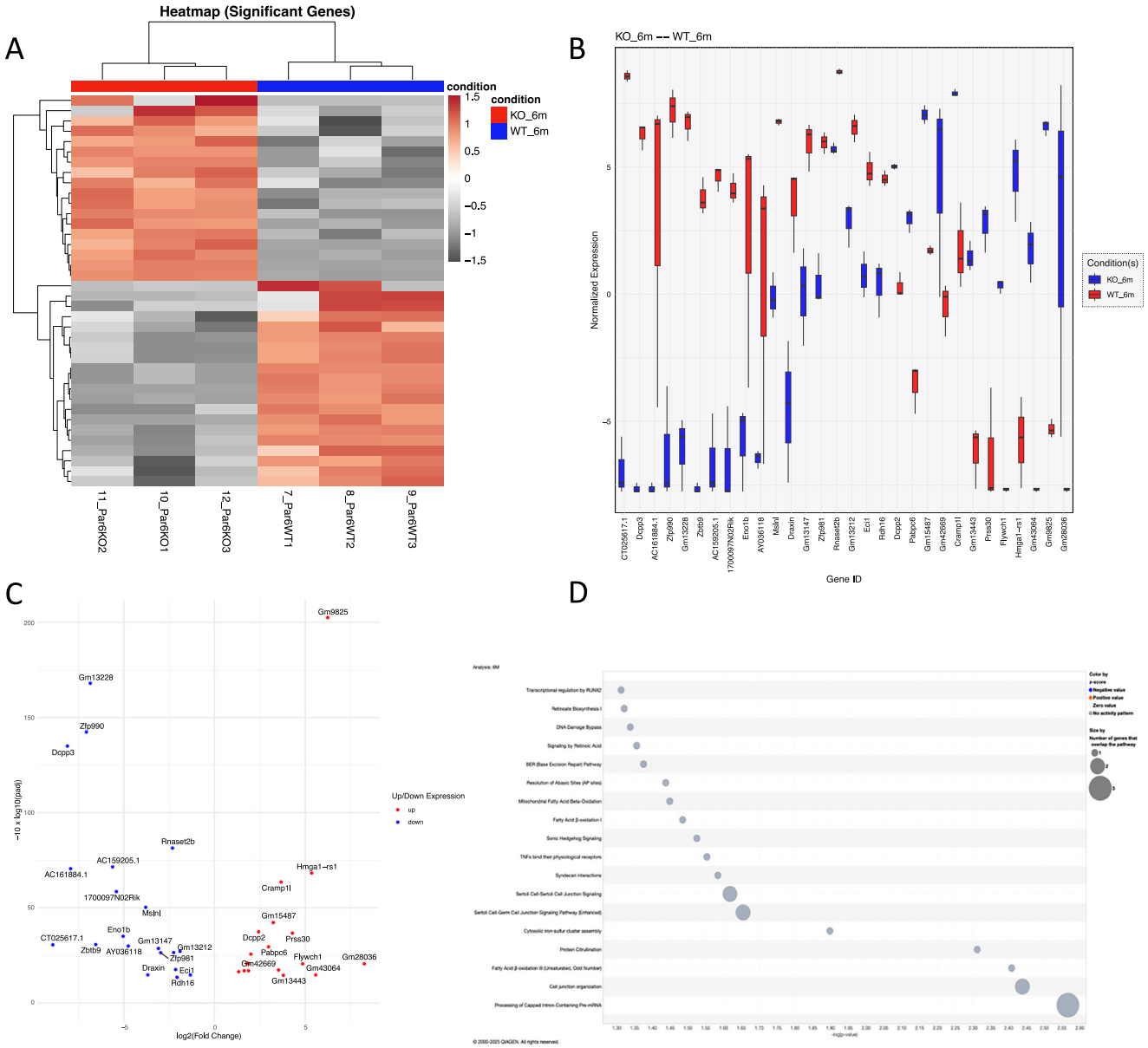


Fig. 4 | Gene expression in Parkin KO oocytes at 6-months-old. A Heatmap illustrating genes differentially expressing between Parkin KO and WT GV oocytes. The color gradient represents normalized expression values, with red indicating higher expression and gray indicating lower expression. **B** Boxplot showing normalized expression levels of the top differentially expressed genes, with red and blue boxes representing WT and KO groups, respectively. **C** Volcano plot showing the distribution of differentially expressed genes between KO and WT oocytes. Each point represents a gene plotted by log2 fold change (x-axis) and -log10 adjusted p-value (y-axis). Red dots indicate significantly upregulated genes in KO and blue dots represent down-regulated genes. The remaining non-significant genes are all plotted as smaller gray points that congregate near the middle of the x axis due to low log2 fold change and low -log 10 adjusted *p* values. **D** Bubble plot of Ingenuity Pathway Analysis (IPA) of RNA-seq data from KO vs WT oocytes, highlighting the top affected pathways. Bubble size represents the number of differentially expressed genes overlapping with each pathway. Color indicates predicted activation state, with gray for statistically enriched but no activity pattern detected pathways.

were approved by the Institutional Animal Care and Use Committee (Protocol #2020-11207). Male mice with a targeted global germline deletion of Parkin were purchased from the Jackson Laboratory (CT, USA) and crossbred with WT females to obtain Parkin heterozygous progeny. These heterozygous males and females were then crossbred to produce both Parkin KO and WT mice. This approach is consistent with the generation and characterization of Parkin KO mice as described by Goldberg and colleagues[43]. In the mouse, the Parkin gene (also known as *Park2*) spans ~1.3 Mb on chromosome 17 and contains 20 exons[44]. Genotyping was performed using established PCR-based protocols. Briefly, DNA was isolated from distal digit samples and amplified with the primer sets recommended by the supplier. In all experiments, female Parkin KO mice were used alongside WT controls.

Assessment of fertility and estrous cycle

To evaluate fertility, female Parkin KO mice ($n = 3$) were paired with proven fertile 12-week-old WT male mice at a 1:1 ratio for 12 weeks. Age-matched WT females ($n = 3$) were similarly bred with WT males under the same conditions. Fertility cages were monitored regularly to document number of litters per female, litter size and total pups per female throughout the study period.

Estrous cycle staging was determined using daily vaginal cytology in 3 WT and 3 KO mice. Vaginal smears were collected once daily between 08:00 and 11:00 AM for a minimum of 10 consecutive days. Vaginal lavage was performed by gently pipetting 10–20 µL sterile phosphate-buffered saline (PBS) into the vaginal opening without penetrating deeply, and the fluid was aspirated back into the tip. This flushing procedure was repeated 2–3 times

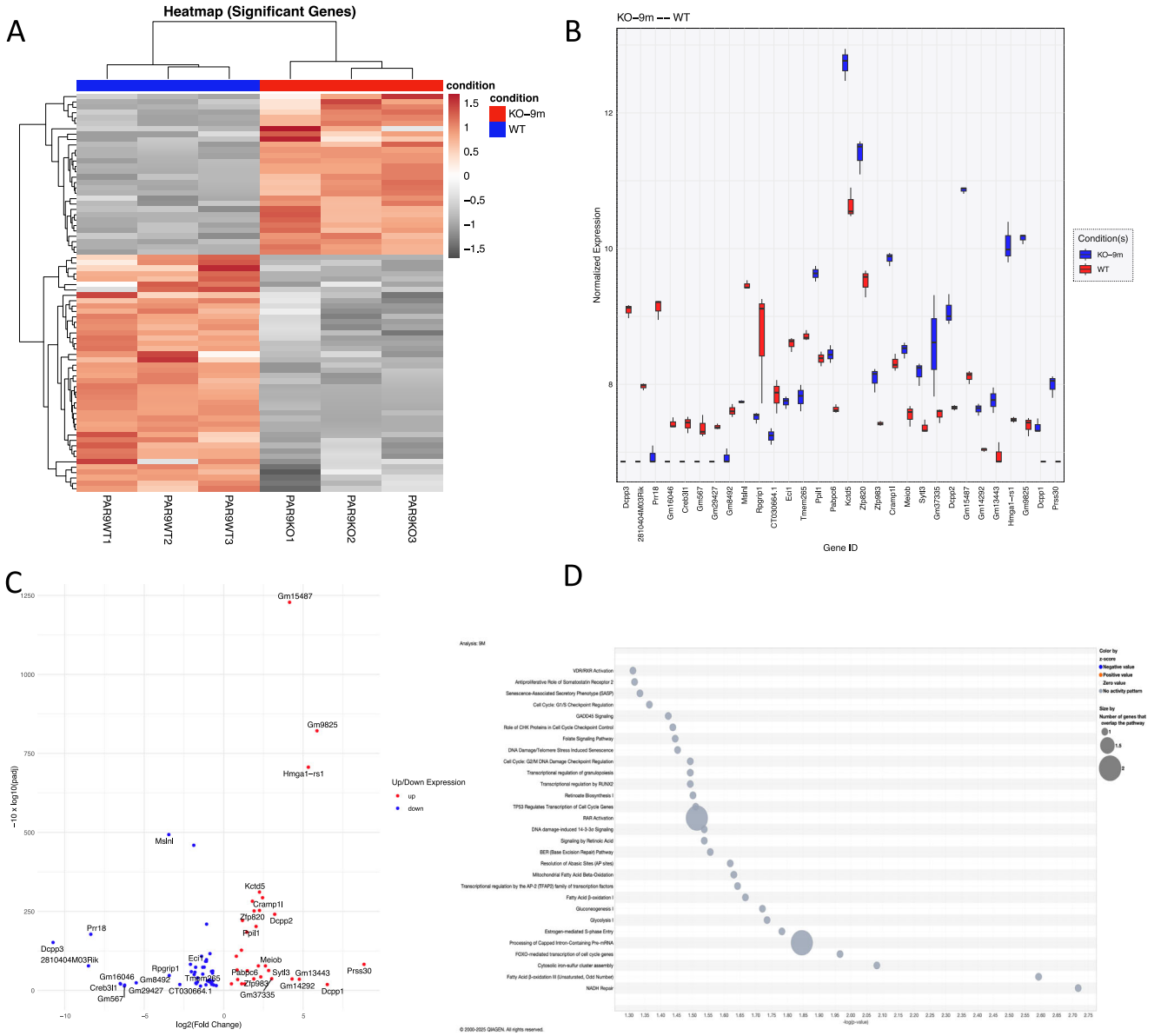


Fig. 5 | Gene expression in Parkin KO oocytes at 9-months-old. A Heatmap illustrating genes differentially expressing between Parkin KO and WT GV oocytes. The color gradient represents normalized expression values, with red indicating higher expression and gray indicating lower expression. **B** Boxplot showing normalized expression levels of the top differentially expressed genes, with red and blue boxes representing WT and KO groups, respectively. **C** Volcano plot showing the distribution of differentially expressed genes between KO and WT oocytes. Each point represents a gene plotted by log2 fold change (x-axis) and -log10 adjusted p-value (y-axis). Red dots indicate significantly upregulated genes in KO and blue dots represent down-regulated genes. The remaining non-significant genes are all plotted as smaller gray points that congregate near the middle of the x axis due to low log2 fold change and low -log 10 adjusted *p* values. **D** Bubble plot of Ingenuity Pathway Analysis (IPA) of RNA-seq data from KO vs WT oocytes, highlighting the top affected pathways. Bubble size represents the number of differentially expressed genes overlapping with each pathway. Color indicates predicted activation state, with gray for statistically enriched but no activity pattern detected pathways.

to obtain sufficient cellular material. The recovered fluid was placed onto labeled glass slides, air-dried, and subsequently stained with 0.1% crystal violet solution for 60 seconds. Slides were rinsed in distilled water and allowed to dry before microscopic evaluation. Samples were examined under light microscopy at 10×–40× magnification. Estrous cycle stage was classified based on the predominant cell type: nucleated epithelial cells (proestrus), anucleate cornified epithelial cells (estrus), mixed leukocytes with cornified and nucleated epithelial cells (metestrus), or leukocyte predominance (diestrus). Staging was performed by an investigator blinded to genotype.

Oocyte collection

Younger (2–3-month old, $n = 3$ per genotype) and older (9–10 months old, $n = 6$ per genotype) female Parkin KO and age-matched WT mice were superovulated. All received an intraperitoneal injection of 10 IU of pregnant mare serum gonadotropin (PMSG, Sigma-Aldrich) to stimulate follicular development. After 44–48 h, GV oocytes were harvested by surgically removing the ovaries and manually dissecting antral follicles in M2 medium (Sigma-Aldrich).

To collect MII oocytes, mice received an additional intraperitoneal injection of 10 IU human chorionic gonadotropin (hCG; Sigma-Aldrich) 48 h after the PMSG injection. MII oocytes were harvested from the oviductal ampullae in M2 medium 16–18 h after hCG injection.

Fertilization

IVF was performed in both Parkin KO and WT mice according to standardized, previously established protocols[28]. Sperm were collected from the cauda epididymides of adult WT male mice into pre-equilibrated

fertilization medium (LifeGlobal) at 37 °C. The suspension was centrifuged at 1200× RPM for 5 min, the supernatant discarded, and the pellet resuspended in fresh medium, following which this wash was repeated. Aliquots of the washed sperm were then placed into pre-equilibrated 200 µl microdrops of fertilization medium under mineral oil and capacitated for 90 min.

MII oocytes (harvested as described above) were then transferred into the sperm-containing drops and co-incubated at 37 °C, 5% CO_2. After 6 h, presumptive zygotes were moved to embryo culture medium (Vitrolife). Fertilization was assessed the following morning by identifying two pronuclei (2PN) zygotes.

Histomorphometric analysis of folliculogenesis in ovaries

To assess folliculogenesis, Parkin KO and WT female mice were superovulated with an intraperitoneal injection of 10 IU PMSG (Sigma-Aldrich). Forty-eight hours later, ovaries were collected, fixed overnight at 4 °C in 4% paraformaldehyde (Sigma-Aldrich) and subsequently transferred to 70% ethanol for storage until processing. Ovaries were then dehydrated, embedded in paraffin, serially sectioned at 5 µm thickness and stained with hematoxylin and eosin. For each ovary, follicles containing oocytes with a visible nucleus on every fifth sections were counted. This was performed by three individual counters to ensure consistency. The follicles were classified as primordial, primary, secondary, early antral, or antral as previously described[29,30]. Briefly, primordial follicles were identified as oocytes surrounded by a single layer of squamous granulosa cells. Primary follicles featured an oocyte encircled by a single layer of cuboidal granulosa cells. Secondary follicles were surrounded by two or more layers of cuboidal granulosa cells. Antral follicles displayed multiple layers of granulosa cells with a clearly visible antral space.

RNA sequencing

GV oocytes were collected from Parkin KO and WT mice at 3, 6, and 9 months of age. Five GV oocytes from individual mice ($n = 3$ mice per genotype per age group) were pooled, totaling 90 samples across three time points (30 samples per age group). Oocytes were lysed and total RNA extracted. Polyadenylated RNA transcripts were reverse transcribed and full-length cDNA was synthesized and amplified using the Smart-seq2 v4 Ultra Low Input RNA Kit (Takara Bio), which optimized for small input amounts such as oocytes. Following amplification, cDNA was purified using AMPure XP beads (Beckman Coulter) to remove residual primers and short fragments. The concentration of amplified cDNA was measured using the Qubit 3.0 Fluorometer (Thermo Fisher Scientific), and fragment size distribution was assessed using the Agilent High Sensitivity D5000 Kit (Agilent Technologies, Santa Clara, CA).

Sequencing libraries were generated using the Nextera® XT DNA Library Preparation Kit and indexed using the Nextera® XT Index Kit (Illumina, San Diego, CA). Libraries were pooled and sequenced on an Illumina HiSeq 2500 platform using 75 bp or 100 bp paired end reads. For RNAseq data analysis, sequencing reads that passed quality filters were demultiplexed and trimmed to remove adapter sequences using Cutadapt. Low quality reads were filtered using FASTX-Toolkit with parameters set to a minimum quality score of 20 and a minimum of 80% high quality bases per read. Clean reads were aligned to the mouse reference genome (GRCm38/mm10) using HiSat2 aligner with default parameters. Differential gene expression analysis between Parkin KO and WT groups was performed using the DESeq2 (version 1.49.4) in R Studio (version 2024.04.0)[45]. Genes were considered differentially expressed if they had a False Discovery Rate (FDR) p-value < 0.05 and an absolute log2 fold change >2. Cluster analysis was conducted using unsupervised hierarchical clustering in R. Pathway enrichment analysis was performed using Ingenuity Pathway Analysis software (QIAGEN IPA, version 81348237, QIAGEN Inc.).

Mitochondrial function

GV oocytes were isolated from KO ($n = 3$) and WT ($n = 3$) 4–5-month-old mice as described above. Mitochondrial ROS was measured with MitoSOX Green Mitochondrial Superoxide Indicator (Thermo Fisher Scientific) according to manufacturer instrctions. A 5 mM stock solution was prepared by dissolving the vial contents in 13 µL of anhydrous DMSO. The stock was diluted by adding 5 µL of 5 mM solution to 50 mL HBSS with calcium and magnesium to yield 500 nM of working solution. GV oocytes were incubated in the MitoSOX for 30 min at 37 °C in the dark, rinsed and immediately imaged live using a Leica DM18 STED confocal microscope under identical imaging settings (laser power, detector gain, pinhole, and exposure time) across groups. For each oocyte, ImageJ (NIH) was used to measure fluorescence pixel intensity (PI) after background subtraction and removal of any artifacts, with per oocyte PI used for statistical analysis.

ΔΨm was assessed with tetramethylrhodamine, methyl ester, perchlorate (TMRM, Thermo Fisher Scientific) following manufacturer's instructions. A 100 µM stock solution was prepared with DMSO and diluted to a 100 nM working concentration in oocyte culture media. GV oocytes were incubated in the TMRM for 30 min at 37 °C in the dark, rinsed, and immediately imaged live using a Leica DM18 STED confocal microscope under identical imaging parameters across groups. For each oocyte, ImageJ (NIH) was used to calculate a fluorescence intensity after background subtraction and exclusion of artifacts, with per oocyte ΔΨm index (arbitrary units) used for analysis.

Statistical analysis

Quantitative data were expressed as mean ± standard error of the mean (SEM). To assess for a significant difference between two groups, unpaired t-tests were performed. Data normality was assessed using the Shapiro–Wilk test prior to applying parametric tests. All statistical analysis were conducted using GraphPad Prism Software (v9). Sample sizes were selected based on prior studies of similar design in reproductive models, which established these sizes as sufficient for detecting relevant biological differences. At least three independent biological replicates were used for each experiment unless otherwise specified.

Data availability

The datasets generated and analyzed during the current study are available from the corresponding author upon request.

Received: 20 June 2025; Accepted: 8 January 2026;
Published online: 22 January 2026

References

1. Esencan, E., Simsek, B. & Seli, E. Analysis of female demographics in the United States: life expectancy, education, employment, family building decisions, and fertility service utilization. *Curr. Opin. Obstet. Gynecol.* **33**, 170–177 (2021).
2. Matthews, T. J. & Hamilton, B. E. Delayed childbearing: more women are having their first child later in life. *NCHS Data Brief.* **21**, 1–8 (2009).
3. Franasiak, J. M. et al. The nature of aneuploidy with increasing age of the female partner: a review of 15,169 consecutive trophectoderm biopsies evaluated with comprehensive chromosomal screening. *Fertil. Steril.* **101**, 656–663 (2014).
4. Seli, E. Ovarian ageing. *Semin. Reprod. Med.* **33**, 375–376 (2015).
5. Chan, D. C. Mitochondria: dynamic organelles in disease, aging, and development. *Cell* **125**, 1241–1252 (2006).
6. Wang, Y., Branicky, R., Noë, A. & Hekimi, S. Superoxide dismutases: Dual roles in controlling ROS damage and regulating ROS signaling. *J. Cell Biol.* **217**, 1915–1928 (2018).
7. Green, D. R., Galluzzi, L. & Kroemer, G. Mitochondria and the autophagy–inflammation–cell death axis in organismal aging. *Science* **333**, 1109–1112 (2011).
8. Kitada, T. et al. Mutations in the parkin gene cause autosomal recessive juvenile parkinsonism. *Nature* **392**, 605–608 (1998).
9. Narendra, D., Tanaka, A., Suen, D. F. & Youle, R. J. Parkin is recruited selectively to impaired mitochondria and promotes their autophagy. *J. Cell Biol.* **183**, 795–803 (2008).

10. Narendra, D. P. & Youle, R. J. The role of PINK1–Parkin in mitochondrial quality control. *Nat. Cell Biol.* **26**, 1639–1651 (2024).
11. Youle, R. J. & Van Der Bliek, A. M. Mitochondrial fission, fusion, and stress. *Science* **337**, 1062–1065 (2012).
12. Chen, G., Kroemer, G. & Kepp, O. Mitophagy: an emerging role in aging and age-associated diseases. *Front. Cell Dev. Biol.* **8**, 200 (2020).
13. Durcan, T. M. & Fon, E. A. The three 'P's of mitophagy: PARKIN, PINK1, and post-translational modifications. *Genes Dev.* **29**, 989–999 (2015).
14. Palikaras, K., Lionaki, E. & Tavernarakis, N. Coordination of mitophagy and mitochondrial biogenesis during ageing in C. elegans. *Nature* **521**, 525–528 (2015).
15. Palikaras, K., Lionaki, E. & Tavernarakis, N. Mechanisms of mitophagy in cellular homeostasis, physiology and pathology. *Nat. Cell Biol.* **20**, 1013–1022 (2018).
16. May-Panloup, P. et al. Low oocyte mitochondrial DNA content in ovarian insufficiency. *Hum. Reprod.* **20**, 593–597 (2005).
17. Van Blerkom, J. Mitochondrial function in the human oocyte and embryo and their role in developmental competence. *Mitochondrion* **11**, 797–813 (2011).
18. Yildirim, R. M. & Seli, E. Mitochondria as determinants of reproductive senescence and competence: implications for diagnosis of embryo competence in assisted reproduction. *Hum. Reprod.* **39**, 2160–2170 (2024).
19. Yildirim, R. M. & Seli, E. The role of mitochondrial dynamics in oocyte and early embryo development. *Semin Cell Dev. Biol.* **159-160**, 52–61(2024).
20. Yildirim, R. M. & Seli, E. Mitochondria as therapeutic targets in assisted reproduction. *Hum. Reprod.* **39**, 2147–2159 (2024).
21. Eura, Y., Ishihara, N., Yokota, S. & Mihara, K. Two mitofusin proteins, mammalian homologues of FZO, with distinct functions are both required for mitochondrial fusion. *J. Biochem.* **134**, 333–344 (2003).
22. Haynes, C. M., Petrova, K., Benedetti, C., Yang, Y. & Ron, D. ClpP mediates activation of a mitochondrial unfolded protein response in C. elegans. *Dev. Cell* **13**, 467–480 (2007).
23. Legros, F., Lombès, A., Frachon, P. & Rojo, M. Mitochondrial fusion in human cells is efficient, requires the inner membrane potential, and is mediated by mitofusins. *Mol. Biol. cell* **13**, 4343–4354 (2002).
24. Wu, G. et al. Mitochondrial unfolded protein response gene CLPP changes mitochondrial dynamics and affects mitochondrial function. *PeerJ* **7**, e7209 (2019).
25. Wang, T. et al. Mitochondrial unfolded protein response gene Clpp is required to maintain ovarian follicular reserve during aging, for oocyte competence, and development of pre-implantation embryos. *Aging Cell* **17**, e12784 (2018).
26. Zhang, M. et al. Mitofusin 1 is required for female fertility and to maintain ovarian follicular reserve. *Cell Death Dis.* **10**, 560 (2019).
27. Zhang, M. et al. Mitofusin 2 plays a role in oocyte and follicle development, and is required to maintain ovarian follicular reserve during reproductive aging. *Aging* **11**, 3919–3938 (2019).
28. Taft, R. In vitro fertilization in mice. *Cold Spring Harb. Protoc.* **2017**, pdb-rot094508 (2017).
29. Myers, M., Britt, K. L., Wreford, N. G., Ebling, F. J. & Kerr, J. B. Methods for quantifying follicular numbers within the mouse ovary. *Reproduction* **127**, 569–580 (2004).
30. Pedersen, T. & Peters, H. Proposal for a classification of oocytes and follicles in the mouse ovary. *Reproduction* **17**, 555–557 (1968).
31. Zhang, X., Wu, X. Q., Lu, S., Guo, Y. L. & Ma, X. Deficit of mitochondria-derived ATP during oxidative stress impairs mouse MII oocyte spindles. *Cell Res.* **16**, 841–850 (2006).
32. Dumollard, R., Carroll, J., Duchen, M. R., Campbell, K. & Swann, K. Mitochondrial function and redox state in mammalian embryos. In *Seminars in cell & developmental biolog*, Vol. 20, 346–353 (Academic Press, 2009).
33. Pasquariello, R. et al. Alterations in oocyte mitochondrial number and function are related to spindle defects and occur with maternal aging in mice and humans. *Biol. Reprod.* **100**, 971–981 (2019).
34. Dorn, I. I. G. W. Central Parkin: the evolving role of Parkin in the heart. *Biochim. Biophys. Acta Bioenerg.* **1857**, 1307–1312 (2016).
35. Rosen, K. M. et al. Parkin protects against mitochondrial toxins and β-amyloid accumulation in skeletal muscle cells. *J. Biol. Chem.* **281**, 12809–12816 (2006).
36. Gong, G. et al. Parkin-mediated mitophagy directs perinatal cardiac metabolic maturation in mice. *Science* **350**, aad2459 (2015).
37. Yun, J. et al. MUL1 acts in parallel to the PINK1/parkin pathway in regulating mitofusin and compensates for loss of PINK1/parkin. *elife* **3**, e01958 (2014).
38. Jin, S. M. et al. Mitochondrial membrane potential regulates PINK1 import and proteolytic destabilization by PARL. *J. Cell Biol.* **191**, 933–942 (2010).
39. Guardia-Laguarta, C. et al. PINK1 content in mitochondria is regulated by ER-associated degradation. *J. Neurosci.* **39**, 7074–7085 (2019).
40. Udagawa, O. et al. Mitochondrial fission factor Drp1 maintains oocyte quality via dynamic rearrangement of multiple organelles. *Curr. Biol.* **24**, 2451–2458 (2014).
41. Narendra, D. P. et al. PINK1 is selectively stabilized on impaired mitochondria to activate Parkin. *PLoS Biol.* **8**, e1000298 (2010).
42. Matsuda, N. et al. PINK1 stabilized by mitochondrial depolarization recruits Parkin to damaged mitochondria and activates latent Parkin for mitophagy. *J. Cell Biol.* **189**, 211–221 (2010).
43. Goldberg, M. S. et al. Parkin-deficient mice exhibit nigrostriatal deficits but not loss of dopaminergic neurons. *J. Biol. Chem.* **278**, 43628–43635 (2003).
44. La Cognata, V. et al. Increasing the coding potential of genomes through alternative splicing: the case of PARK2 gene. *Curr. Genom* **15**, 203–216 (2014).
45. Love, M. I., Huber, W. & Anders, S. Moderated estimation of fold change and dispersion for RNA-seq data with DESeq2. *Genome Biol.* **15**, 1–21 (2014).

Acknowledgment

This work was supported by a grant from Foundation for Embryonic Competence to ES. ARE was supported by a grant by the Instituto de Salud Carlos III and co-funded by the European Union (Fondo Social Europeo), "El FSE invierte en tu futuro" (PI21/00305 [IC]); the Generalitat Valenciana, (CIPROM/2021/058 [IC]); the Spanish Ministry of Science, Innovation and Universities (CNS2024-154767 [IC], FPU19/04850 [ARE]); and by a US–Spain Fulbright grant (ARE).

Author contributions

M.V. performed experiments such as oocyte collection, IVF and histomorphometric follicle counting, mitochondrial function testing, maintained the mouse colony, and wrote the manuscript. A.R.E. and Y.E. established the colony and performed experiments including oocyte quantification and histomorphometric follicle counting. R.M.Y. performed oocyte collection and participated in the generation of RNA sequencing results. G.N.S. performed experiments including oocyte collection, IVF and histomorphometric follicle counting, mitochondrial function testing. R.G.M. and S.M. participated in RNA sequencing, pathway analysis and manuscript writing. L.T. contributed to colony maintenance and histomorphometric follicle counting. I.C. contributed to review of results and manuscript writing. R.S. provided oversight for the project and contributed to manuscript writing. E.S. supervised the project and provided oversight on study design, data interpretation and manuscript writing.

Competing interests
The authors declare no competing interests.

Additional information
Supplementary information The online version contains supplementary material available at https://doi.org/10.1038/s41514-026-00332-6.

Correspondence and requests for materials should be addressed to Emre Seli.

Reprints and permissions information is available at http://www.nature.com/reprints

Publisher's note Springer Nature remains neutral with regard to jurisdictional claims in published maps and institutional affiliations.

Open Access This article is licensed under a Creative Commons Attribution-NonCommercial-NoDerivatives 4.0 International License, which permits any non-commercial use, sharing, distribution and reproduction in any medium or format, as long as you give appropriate credit to the original author(s) and the source, provide a link to the Creative Commons licence, and indicate if you modified the licensed material. You do not have permission under this licence to share adapted material derived from this article or parts of it. The images or other third party material in this article are included in the article's Creative Commons licence, unless indicated otherwise in a credit line to the material. If material is not included in the article's Creative Commons licence and your intended use is not permitted by statutory regulation or exceeds the permitted use, you will need to obtain permission directly from the copyright holder. To view a copy of this licence, visit http://creativecommons.org/licenses/by-nc-nd/4.0/.

© The Author(s) 2026